Chemistry of Metals and Alloys

Chem. Met. Alloys 17 (2024) 5-12
Ivan Franko National University of Lviv
http://publications.lnu.edu.ua/chemetal

Isothermal section of the Er–Ni–Sb ternary system at 1073 K

L. ROMAKA[1]*, Yu. STADNYK[1], P. KLYZUB[1]

[1] *Department of Inorganic Chemistry, Ivan Franko National University of Lviv, Kyryla i Mefodiya St. 6, 79005 Lviv, Ukraine*
* *Corresponding author. E-mail: lyubov.romaka@gmail.com*

Received March 15, 2024; accepted July 1, 2024
https://doi.org/10.30970/cma17.0439

The interaction between the components in the ternary system Er–Ni–Sb was investigated by X-ray diffraction, microstructural analysis, and energy-dispersive X-ray spectroscopy in the full concentration range at 1073 K. At this temperature, the Er–Ni–Sb system is characterized by the existence of two ternary compounds: ErNiSb (structure type MgAgAs, space group *F*-43*m*, *a* = 0.62673(1) nm) and Er_5Ni_2Sb (structure type Mo_5SiB_2, space group *I*4/*mcm*, *a* = 0.7518(2), *c* = 1.3287(6) nm). The antimonide ErNiSb is characterized by a homogeneity range that extends from 33 to 28 at.% Ni. The binary compound (NaCl structure type) ErSb dissolves up to ~14 at.% Ni, filling the vacant 8*c* site in the structure of ErSb by smaller Ni atoms. The substitution-type solid solution $Er_5Ni_xSb_{3-x}$ (Yb_5Sb_3-type) extends to about 6 at.% Ni.

Intermetallics / Phase diagram / X-ray diffraction / Scanning electron microscopy

1. Introduction

Intermetallic compounds with the structure type MgAgAs (so-called half-Heusler phases) are characterized by semiconductor properties and are used as starting materials for the production of thermoelectric materials. Among the numerous half-Heusler phases, *R*NiSb antimonides (*R* is a rare-earth metal) attract considerable interest because of the coexistence of magnetism and semiconducting behavior [1-4].

According to literature data, equiatomic *R*NiSb compounds form for the full row of rare earths [1,5-7]. In the case of the light rare-earth metals, depending on the method of synthesis, the *R*NiSb antimonides crystallize in different structure types – AlB_2, BeZrSi (*R* = La, Ce, Pr, Nd, Sm), or TiNiSi (*R* = La). The half-Heusler *R*NiSb phases with rare-earth metals of the yttrium subgroup crystallize in the structure type MgAgAs (space group *F*-43*m*). Two structural variants are known for the GdNiSb antimonide – a high-temperature modification with a hexagonal structure (structure type AlB_2) and a low-temperature modification with a MgAgAs-type structure [5].

Experimental studies of the interaction of the components in metallic systems is an important step to obtain information regarding the peculiarities of the formation, temperature and concentration stability, and crystal structures of intermediate phases for further studies of the physical properties of intermetallics. The ternary system Er–Ni–Sb has previously been studied at 773 K [8], where the formation of the ternary compounds Er_5Ni_2Sb (structure type Mo_5B_2Si) and ErNiSb (structure type MgAgAs) was confirmed. According to the reported data [8] both compounds are characterized by point compositions. A study of the Er–Ni–Sb system at 1073 K in the Er-rich region [9] revealed the formation of two ternary compounds: the already known compound Er_5Ni_2Sb (Mo_5B_2Si-type structure) and the new compound $Er_5Ni_xSb_{3-x}$ with Yb_5Sb_3-type structure. Further studies of the interaction of the components in the related {Y, Gd, Lu}–Ni–Sb systems [10,11] disclosed that the half-Heusler phases *R*NiSb are characterized by a homogeneity range extending from the equiatomic composition to a composition with a lower nickel content.

In this contribution we report the results of an experimental investigation of the isothermal section at 1073 K of the phase diagram of the ternary system Er–Ni–Sb in the full concentration range.

2. Experimental

To construct the phase equilibrium diagram of the ternary system Er–Ni–Sb, polycrystalline samples were synthesized by direct arc melting the constituent

metals (erbium, purity 99.9 wt.%, nickel, purity 99.99 wt.%, antimony, purity 99.999 wt.%) in a protective argon atmosphere with a non-consumable tungsten electrode on a water-cooled copper hearth. To remove traces of impurities, a Ti ingot was first melted as a getter. To compensate for evaporative losses of antimony during the arc melting, 2-3 wt.% (depending on the sample composition) excess Sb was added. For better homogenization, the alloys were re-melted twice. After melting, the overall weight losses of the alloys were generally less than 1 wt.%. Pieces of the arc-melted ingots were then placed in evacuated quartz ampoules and annealed at 1073 K for 700 h. The annealed ingots were removed from the furnace and quenched in cold water.

Powder X-ray diffraction was used for the construction of the phase diagram (determination of the phase fields, identification of intermediate phases, formation of solid solutions). The observed diffraction intensities of the powder patterns (DRON-2.0, Fe *K*α radiation) were compared with reference powder patterns of the constituent elements and known binary and ternary phases (program PowderCell [12]). Elemental and phase compositions of the prepared samples were examined by Scanning Electron Microscopy (SEM) using a Tescan Vega 3 LMU scanning microscope with a Link EDX system operated at 20 kV and 60 μA. Quantitative electron probe microanalysis (EPMA) of the phases was carried out using an energy-dispersive X-ray analyzer with the pure elements as standards (typical acceleration voltage was 20 kV; *K*- and *L*-lines were used). For each phase, 3-5 measurements were made to obtain an average value.

Refinements of the crystallographic parameters were performed using the WinCSD [13] program package.

3. Results and discussion

3.1 Binary boundary systems

The binary systems that delimit the ternary Er–Ni–Sb system have been investigated previously. The binary compounds are briefly described below.

Er–Sb. The Er–Sb phase diagram was reported in [14]. Three compounds were found: Er_5Sb_3, ErSb, and $ErSb_2$. ErSb melts congruently, Er_5Sb_3 and $ErSb_2$ are formed by peritectic reactions. Two polymorphic forms of the Er_5Sb_3 binary were studied in [9]. It was found that the low-temperature form belongs to the hexagonal Mn_5Si_3-type, while the high-temperature modification crystallizes in the orthorhombic structure type β-Yb_5Sb_3. Additionally, Er_3Sb_4 with Th_3P_4-type structure was reported in [15].

Er–Ni. The phase diagram as assessed in compilations [16,17] was used for our investigation. Nine binary phases form at 1073 K in the Er–Ni system: Er_3Ni (Fe_3C-type), Er_3Ni_2 (Er_3Ni_2-type), ErNi (FeB-type), $ErNi_2$ ($MgCu_2$-type), $ErNi_3$ ($PuNi_3$-type), Er_2Ni_7 (Gd_2Co_7-type), $ErNi_4$ ($PuNi_4$-type), $ErNi_5$ ($CaCu_5$-type), and Er_2Ni_{17} (Th_2Ni_{17}-type).

Ni–Sb. The version of this well-known phase diagram accepted here was taken from [16,17]. According to the reported data, four binary compounds form in this system: Ni_3Sb (high-temperature phase with Bi_3F-type, low-temperature phase with Cu_3Ti-type), Ni_5Sb_2 (own structure type), NiSb (NiAs-type), and $NiSb_2$ (FeS_2-type). The high-temperature phase Ni_3Sb and NiSb have significant homogeneity ranges. Crystallographic characteristics of the binary compounds in the Er–Sb, Er–Ni and Ni–Sb systems at 1073 K are gathered in Table 1.

Table 1 Binary phases relevant to the 1073 K isothermal section of the Er–Ni–Sb system*.

Phase	Melting and transformation temperature	Pearson symbol, structure type	Lattice parameters, nm			Ref.
			a	*b*	*c*	
ErSb	m 2313 K	*cF*8, NaCl	0.6115(3)	–	–	This work
Er_5Sb_3	p 1913 K	*oP*32, Yb_5Sb_3	1.1698(3)	0.9128(3)	0.8022(1)	This work
Er_3Ni	p 1118 K	*oP*16, Fe_3C	0.6804	0.9430	0.6245	[18]
Er_3Ni_2	p 1073 K	*hR*45, Er_3Ni_2	0.8472	–	1.5680	[18]
ErNi	m 1373 K	*oP*8, FeB	0.7021(4)	0.4120(3)	0.54141(2)	This work
$ErNi_2$	p 1528 K	*cF*24, $MgCu_2$	0.7055(3)	–	–	This work
$ErNi_3$	p 1593 K	*hR*36, $PuNi_3$	0.4941	–	2.4252	[19]
Er_2Ni_7	pd 1548 K	*hP*36, Ce_2Ni_7	0.4951	–	2.4210	[19]
$ErNi_5$	pd 1653 K	*hP*6, $CaCu_5$	0.4856(3)	–	0.3960(2)	This work
Er_2Ni_{17}	p 1588 K	*hP*38, Th_2Ni_{17}	0.8287	–	0.8017	[18]
Ni_3Sb	m 1434 K	*cF*16, Bi_3F	0.5930	–	–	[20]
NiSb	m 1423 K	*hP*4, NiAs	0.3987(3)	–	0.5199(4)	This work

*p – peritectic reaction; m – melting; pd – peritectoid reaction

3.2 Isothermal section of the Er–Ni–Sb system

To study the phase relations in the Er–Ni–Sb system, 36 ternary and binary alloys were prepared, annealed at 1073 K and examined by XRPD and EPMA. Based on the results, the isothermal section of the phase diagram of the Er–Ni–Sb system was constructed over the whole concentration range (Fig. 1). As regards the boundary systems, the presence of almost all the binary compounds reported in the Er–Ni, Er–Sb, and Ni–Sb systems was confirmed at 1073 K (Fig. 1, Table 1).

Two binaries, Ni_3Sb (high-temperature phase) and NiSb, were confirmed in the Ni–Sb system. The homogeneity ranges at 1073 K of these compounds were determined based on the data of EPM analysis and are limited by the compositions $Ni_{74.31}Sb_{25.69}$ – $Ni_{69.74}Sb_{30.26}$ (for Ni_3Sb), and $Ni_{55.36}Sb_{44.64}$ – $Ni_{48.06}Sb_{51.91}$ (for NiSb). In the Er–Sb binary system the existence of two compounds, ErSb and Er_5Sb_3, was confirmed. At the temperature of investigation Er_5Sb_3 crystallizes with orthorhombic structure type Yb_5Sb_3, which, according to [9], represents the high-temperature modification. In the Er–Ni system, the binary compound $ErNi_4$ ($PuNi_4$-type) was not observed. In the original report [18], this compound was prepared by induction melting.

As shown in Fig. 1, the isothermal section of the Er–Ni–Sb system at 1073 K consists of 17 three-phase, 32 two-phase, and 15 single-phase regions. Most of the solid-state equilibria (9) are formed by the ternary antimonide ErNiSb. Phase compositions of selected alloys are presented in Table 2. Microphotographs of some alloys are shown in Figs. 2 and 3.

Table 2 Phase composition of selected alloys from the Er–Ni–Sb system.

Nominal composition/ composition from EPMA data, at.%	Phase	Structure type	Lattice parameters, nm			EPMA data, at.%		
			a	*b*	*c*	Er	Ni	Sb
$Er_{30}Ni_{60}Sb_{10}$	$ErNi_2$	$MgCu_2$	0.7126(3)	–	–	–	–	–
	$ErNi_3$	$PuNi_3$	0.4962(3)	–	2.4136(4)	–	–	–
	ErNiSb	MgAgAs	0.6267(2)	–	–	–	–	–
$Er_{65}Ni_{20}Sb_{15}$	Er_3Ni	Fe_3C	0.6793(3)	0.9435(4)	0.6238(4)	75.81	23.93	0.26
$Er_{64.57}Ni_{20.12}Sb_{15.31}$	(Er)	Mg	0.3559(3)	–	0.5578(4)	100.0	–	–
	$Er_5Ni_xSb_{3-x}$	Yb_5Sb_3	1.1712(2)	0.9050(3)	0.7924(4)	62.24	6.32	31.44
$Er_{60}Ni_{20}Sb_{20}$	Er_5Ni_2Sb	Mo_5SiB_2	0.7517(4)	–	1.3286(6)	62.27	25.75	11.98
$Er_{60.33}Ni_{19.98}Sb_{19.69}$	ErNi	FeB	0.7020(4)	0.4119(4)	0.5414(3)	49.67	49.55	0.78
	$Er_5Ni_xSb_{3-x}$	Yb_5Sb_3	1.1652(6)	0.9106(4)	0.7912(4)	62.33	6.26	31.41
$Er_{55}Ni_{30}Sb_{15}$	$Er_5Ni_xSb_{3-x}$	Yb_5Sb_3	1.1652(5)	0.9107(6)	0.7911(3)	62.19	6.49	31.32
$Er_{54.36}Ni_{31.07}Sb_{14.57}$	ErNi	FeB	0.7021(4)	0.4121(3)	0.5414(4)	50.90	47.72	1.38
$Er_{30}Ni_{45}Sb_{25}$	ErNiSb	MgAgAs	0.6269(2)	–	–	33.02	33.60	33.38
$Er_{29.36}Ni_{46.07}Sb_{24.57}$	$ErNi_5$	$CaCu_5$	0.4857(3)	–	0.3968(3)	16.93	81.28	1.79
$Er_{35}Ni_{35}Sb_{30}$	ErNiSb	MgAgAs	0.6257(2)	–	–	35.69	28.69	35.62
$Er_{34.18}Ni_{34.83}Sb_{30.99}$	$ErNi_2$	$MgCu_2$	0.7126(2)	–	–	31.93	67.30	0.77
$Er_{45}Ni_{20}Sb_{35}$	$ErNi_xSb$	NaCl	0.6111(2)	–	–	45.59	7.55	46.86
$Er_{44.04}Ni_{21.13}Sb_{35.83}$	Er_5Sb_3	Yb_5Sb_3	1.1699(5)	0.9107(6)	0.7934(8)	61.28	3.42	35.30
	$ErNi_2$	$MgCu_2$	0.7128(2)	–	–	30.95	67.47	1.58
$Er_{62}Ni_3Sb_{35}$	$ErNi_xSb$	NaCl	0.6111(2)	–	–	47.14	4.85	48.01
$Er_{61.59}Ni_{2.40}Sb_{36.01}$	Er_5Sb_3	Yb_5Sb_3	1.1680(6)	0.9134(6)	0.8003(7)	61.96	2.56	35.48
$Er_{15}Ni_{50}Sb_{35}$	ErNiSb	MgAgAs	0.6268(2)	–	–	32.80	33.08	34.12
$Er_{14.33}Ni_{51.20}Sb_{34.47}$	NiSb	NiAs	0.3927(2)	–	0.5132(3)	0.67	53.98	45.35
	Ni_3Sb	BiF_3	Not determined			0.36	69.78	29.86
$Er_{20}Ni_{40}Sb_{40}$	ErNiSb	MgAgAs	0.62681(2)	–	–	–	–	–
	NiSb	NiAs	0.3925(3)	–	0.5133(3)	–	–	–
$Er_{30}Ni_{30}Sb_{40}$	ErNiSb	MgAgAs	0.6258(2)	–	–	–	–	–
	$ErNi_xSb$	NaCl	0.6119(2)	–	–	–	–	–
	NiSb	NiAs	0.3936(3)	–	0.5139(4)	–	–	–
$Er_{40}Ni_{20}Sb_{40}$	ErNiSb	MgAgAs	0.6257(2)	–	–	36.08	28.58	35.34
$Er_{39.33}Ni_{21.20}Sb_{39.47}$	$ErNi_xSb$	NaCl	0.6119(3)	–	–	42.96	13.63	43.41
	$ErNi_2$	$MgCu_2$	0.7127(3)	–	–	31.84	66.83	1.33
$Er_{26}Ni_{26}Sb_{48}$	$ErNi_xSb$	NaCl	0.6111(2)	–	–	44.54	10.25	45.21
$Er_{26.83}Ni_{26.11}Sb_{47.06}$	NiSb	NiAs	0.3935(3)	–	0.5136(3)	0.62	50.28	49.10

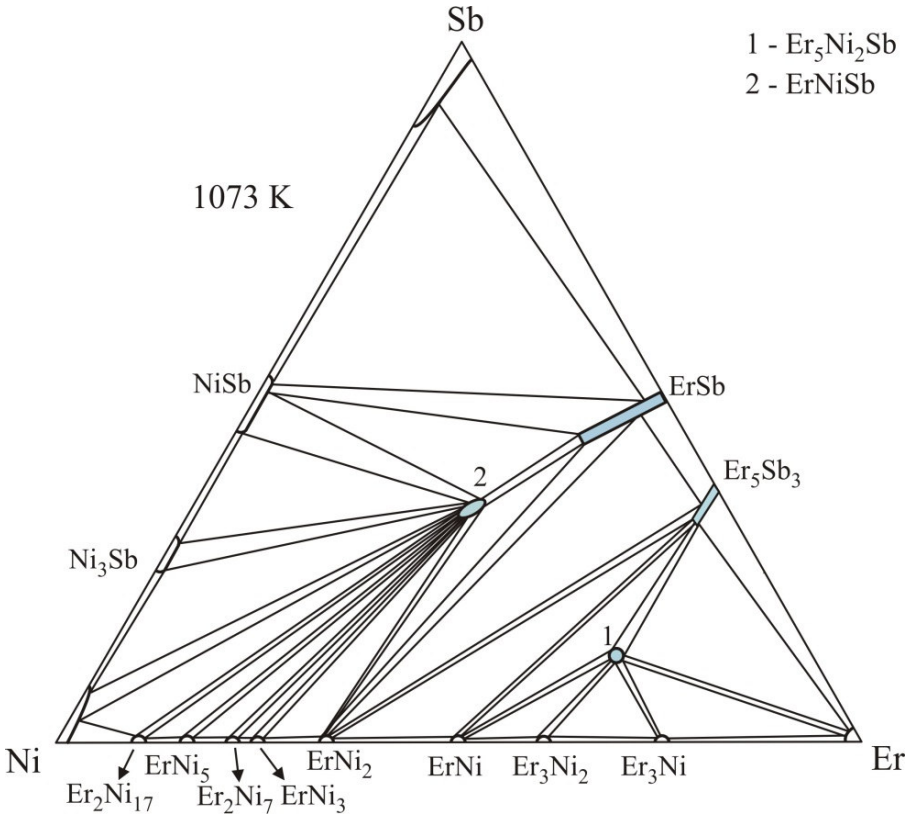

Fig. 1 Isothermal section of the Er–Ni–Sb system at 1073 K.

At the temperature of investigation, 1073 K, the existence of the two known ternary compounds ErNiSb and Er_5Ni_2Sb [5,21] was confirmed in the Er–Ni–Sb system. Crystallographic characteristics of the ternary compounds observed in the Er–Ni–Sb system are given in Table 3.

For the ErNiSb half-Heusler compound, similarly to the previously studied *R*NiSb compounds (*R* = Y, Gd, Lu) [10,11], the existence of a homogeneity range in the direction of lower nickel content was found. The homogeneity range of the $ErNi_{1-x}Sb$ half-Heusler phase extends from 33 to 28 at.% of Ni towards the $ErNi_xSb$ solid solution (Fig. 1). According to the results of the EPM analysis, the homogeneity range is limited by the compositions $Er_{32.80}Ni_{33.08}Sb_{34.12}$ and $Er_{35.69}Ni_{28.69}Sb_{35.62}$. The sample $Er_{40}Ni_{25}Sb_{35}$ contained the phases $ErNi_xSb$ and $ErNi_{1-x}Sb$ in equilibrium with binary $ErNi_2$ (Fig. 3a).

The formation of the earlier reported compound $ErNiSb_2$ ($HfCuSi_2$-type) [22] was not confirmed under the experimental conditions used in our work. The sample of the corresponding composition contained the binary compound NiSb and $ErNi_xSb$ in equilibrium (Fig. 2a). In [22] the antimonide $ErNiSb_2$ was prepared using Sb as a flux and the crystal structure was investigated by single-crystal diffraction.

The compound $ErNi_{1.5}Sb_2$ was synthesized by induction melting of metal powders [23]. The authors noted that the compound is characterized by a defective structure and crystallizes in the $CaBe_2Ge_2$ structure type. Further studies of isostructural compounds revealed that these compounds in fact belong to the monoclinic structure type $Y_3Ni_{5.8}Sb_5$ (space group $P2_1/m$) [24]. During our study of this part of the Er–Ni–Sb system, samples annealed at 1073 K were examined by X-ray diffraction and energy-dispersive X-ray spectroscopy. According to the obtained results the corresponding samples belong to two- or three-phase regions and contain the ternary compound ErNiSb in equilibrium either with NiSb or with the binary compounds NiSb and Ni_3Sb (Fig. 3c). According to the phase analysis the sample $Er_{20}Ni_{40}Sb_{40}$ contained as main phase ErNiSb, in equlibrium with NiSb (Fig. 4a). However, the compound $ErNi_2Sb_2$ was identified in as-cast samples. The powder pattern of the as-cast sample $Er_{20}Ni_{40}Sn_{40}$ was indexed on the basis of a tetragonal lattice ($CaBe_2Ge_2$ structure type) with cell parameters $a = 0.4198(1)$, $c = 0.9619(2)$ nm. Unfortunately, the as-cast sample contained in addition significant amounts of ErNiSb and NiSb (Fig. 4b). This indicates that other methods of synthesis should be used to prepare this compound.

The solubility of the third component in the binary compounds of the Ni–Sb and Er–Ni systems under the conditions used here is not significant (up to 1.5-2 at.%). In order to determine the solubility of Ni

in the ErSb binary, several alloys along the line between ErNiSb and ErSb were prepared and examined. It was found that the binary compound ErSb (NaCl structure type) dissolves up to ~14 at.% Ni, partly filling the vacant 8*c* site in the structure by the smaller Ni atoms. According to EPMA data, the limiting composition of the $ErNi_xSb$ solid solution is $Er_{42.96}Ni_{13.63}Sb_{43.41}$. The lattice parameter changes from $a = 0.6109(2)$ (for ErSb) to $a = 0.6118(2)$ nm (for the $Er_{43}Ni_{14}Sb_{43}$ sample).

Taking into account the data concerning the formation of two modifications of the Er_5Sb_3 binary [9], we prepared a sample of the corresponding composition by arc melting and annealing at 1073 K for 700 h. Phase analysis of the annealed Er_5Sb_3 sample clearly showed the presence of the orthorhombic modification with structure type Yb_5Sb_3 ($a = 1.1698(3)$, $b = 0.9128(3)$, $c = 0.8022(1)$ nm, $V = 0.856(5)$ nm^3). In the ternary part of the Er–Ni–Sb system a substitution-type solid solution $Er_5Ni_xSb_{3-x}$ was formed along the isoconcentrate ~63 at.% Er up to about 6 at.% Ni ($a = 1.1767(8)$, $b = 0.9027(6)$, $c = 0.7910(3)$ nm, $V = 0.840(2)$ nm^3 for the sample $Er_{63}Ni_6Sb_{31}$) (Fig. 1). The limiting composition of the $Er_5Ni_xSb_{3-x}$ solid solution was confirmed by EPMA data ($Er_{62.47}Ni_{6.81}Sb_{30.72}$) (Fig. 2c). An analogous solid solution was observed in the previously studied Tm–Ni–Sb system [11]. In contrast to our data, Zelinska *et al.* [9] presented the $Er_5Ni_xSb_{3-x}$ phase as an individual phase. The discrepancy between the data obtained in our work and those reported in [9] may be due to different methods of preparation.

Table 3 Crystallographic characteristics of the ternary compounds in the Er–Ni–Sb system.

Compound	Structure type	Space group	Lattice parameters, nm		
			a	*b*	*c*
ErNiSb	MgAgAs	*F*-43*m*	0.62673(1)	–	–
Er_5Ni_2Sb	Mo_5SiB_2	*I*4/*mcm*	0.7518(2)	–	1.3287(6)
$ErNi_2Sb_2$ (as-cast sample)	$CaBe_2Ge_2$	*P*4/*nmm*	0.4198(1)	–	0.9619(2)

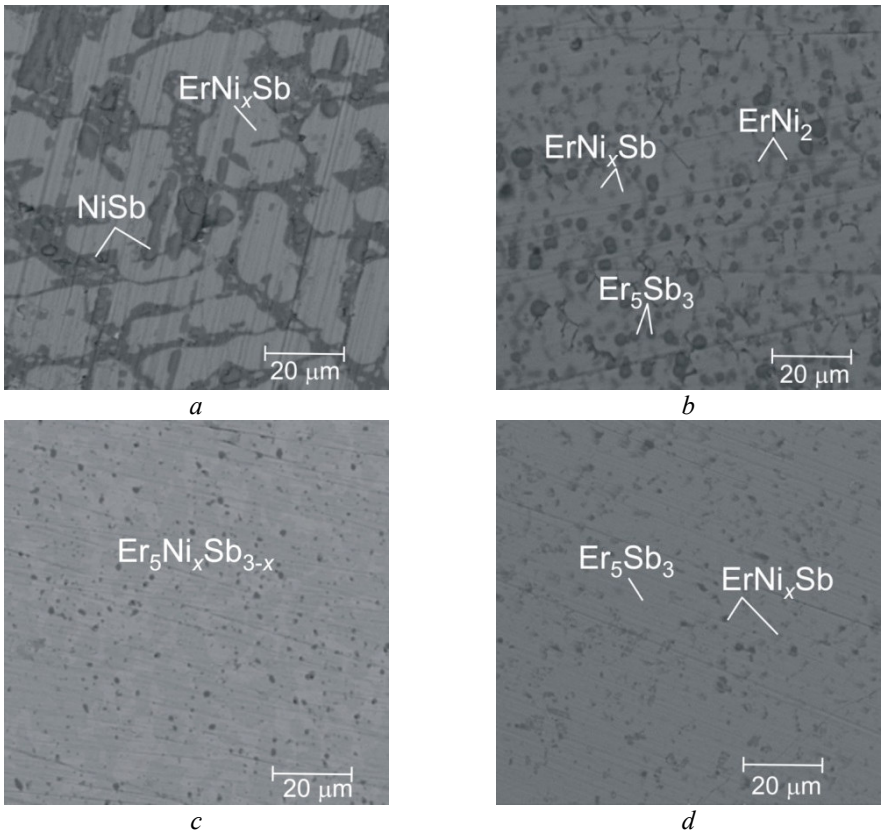

Fig. 2 SEM images of alloys from the Er–Ni–Sb system: *a*) $Er_{26}Ni_{26}Sb_{48}$; *b*) $Er_{45}Ni_{20}Sb_{35}$; *c*) $Er_{62}Ni_6Sb_{32}$; *d*) $Er_{62}Ni_3Sb_{35}$.

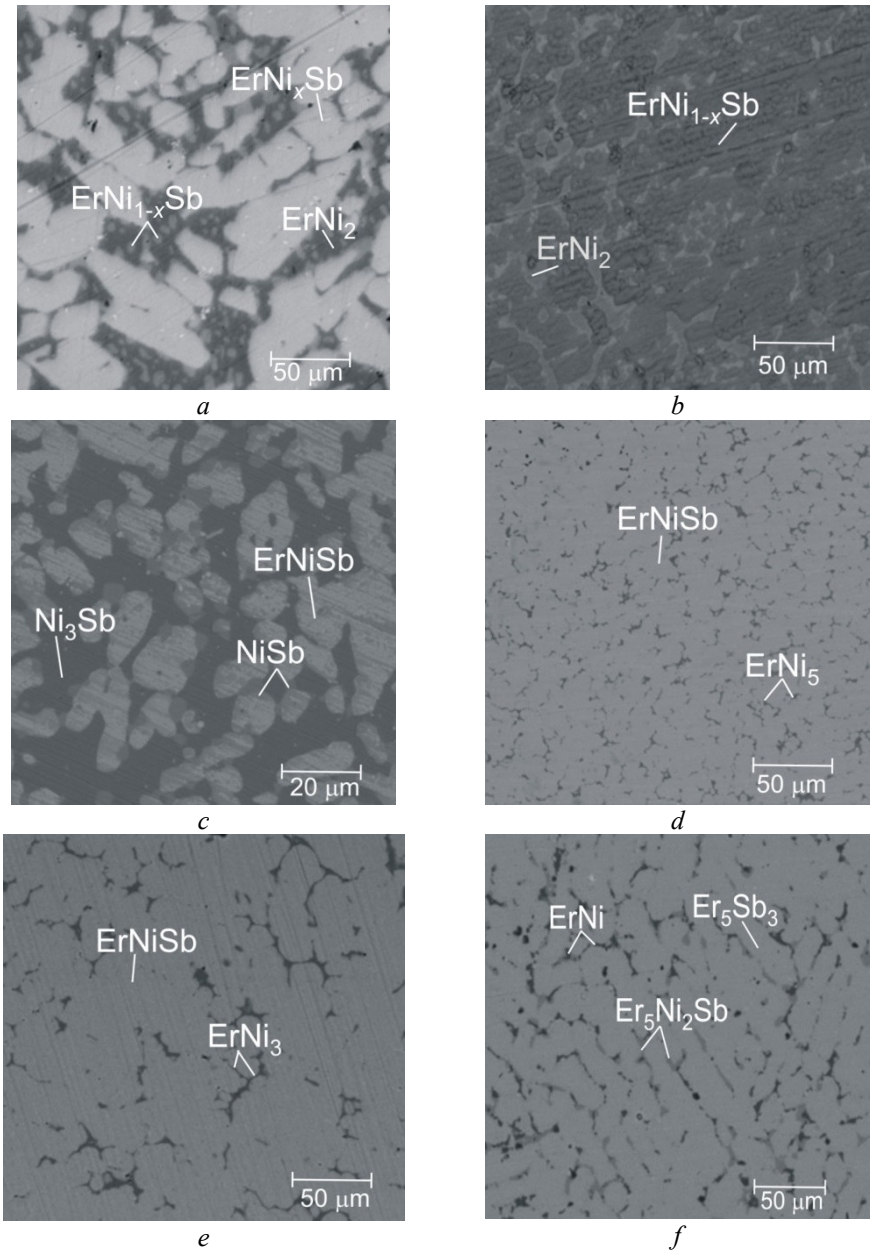

Fig. 3 SEM pictures of alloys from the Er–Ni–Sb system: *a*) $Er_{40}Ni_{25}Sb_{35}$; *b*) $Er_{35}Ni_{35}Sb_{30}$; *c*) $Er_{15}Ni_{50}Sb_{35}$; *d*) $Er_{30}Ni_{45}Sb_{25}$; *e*) $Er_{33}Ni_{35}Sb_{32}$; *f*) $Er_{30}Ni_{45}Sb_{25}$.

Despite the different temperatures, some similarities can be noted between the Er–Ni–Sb system studied at 1073 K in this work and the previous investigation of the same system at 773 K [8]. In particular, the two ternary compounds ErNiSb and Er_5Ni_2Sb form at both temperatures. The most remarkable differences between the two phase diagrams concern the extended $ErNi_xSb$ solid solution and the homogeneity range of the ErNiSb half-Heusler phase, which were not observed at 773 K.

4. Conclusions

Based on X-ray powder diffraction and energy-dispersive X-ray spectroscopy, the phase diagram of the Er–Ni–Sb system was constructed at 1073 K in the whole concentration range. It was established that at this temperature the system is characterized by the existence of two ternary compounds, ErNiSb and Er_5Ni_2Sb. The experimental results revealed that an $Er_5Ni_xSb_{3-x}$ substitutional solid solution, rather than an individual ternary compound $Er_5Ni_xSb_{3-x}$, forms in the system. The occurrence of the earlier reported $ErNiSb_2$ compound was not confirmed under the conditions used here. The solubility limit of Ni in the binary compound ErSb was found to be ~14 at.%. A homogeneity range was established for the ErNiSb half-Heusler phase; it extends from 33 to 28 at.% Ni and plays an important role for transport properties.

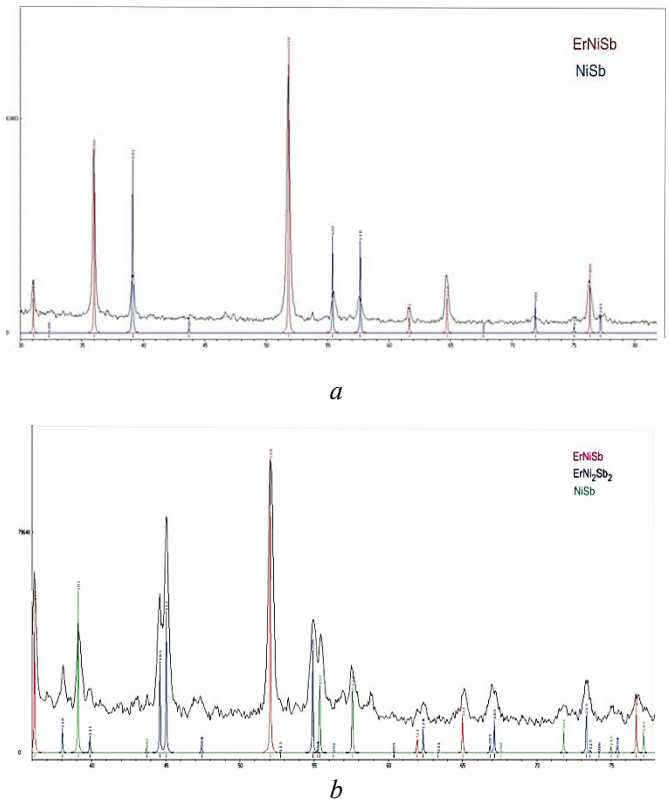

Fig. 4 X-ray powder patterns of the $Er_{20}Ni_{40}Sb_{40}$ sample: *a*) annealed at 1073 K, *b*) as-cast.

It should be noted that the thermoelectric properties of half-Heusler intermetallics in many cases are strongly dependent on the microstructure, heat treatments, homogeneity domains, and atomic disorder. Previous investigations of (Y, Gd, Lu)NiSb half-Heusler phases [10,11] revealed their off-stoichiometry, which has a noticeable impact on the thermoelectric properties. Doping the initial half-Heusler phases with other elements would also help in the synthesis of multicomponent materials (solid solutions).

References

[1] R.V. Skolozdra, A. Guzik, A.M. Goryn, J. Pierre, *Acta Phys. Pol.* 92 (1997) 343-346.

[2] I. Karla, J. Pierre, B. Ouladdiaf, *Physica B* 253(3) (1998), 215-221. https://doi.org/10.1016/S0921-4526(98)00394-9

[3] I. Karla, J. Pierre, A.P. Murani, M. Neumann, *Physica B* 271 (1999) 294-303. https://doi.org/10.1016/S0921-4526(99)00196-9

[4] T. Sekimoto, K. Kurosaki, H. Muta, S. Yamanaka, *J. Appl. Phys*. 99 (2006) 103701-1. https://doi.org/10.1063/1.2196109

[5] K. Hartjes, W. Jeitschko, *J. Alloys Compd*. 226 (1995) 81-86. https://doi.org/10.1016/0925-8388(95)01573-6.

[6] I. Karla, J. Pierre, R.V. Skolozdra, *J. Alloys Compd.* 265 (1998) 42-48. https://doi.org/10.1016/S0925-8388(97)00419-2.

[7] L. Menon, S.K. Malik, *Phys. Rev. B* 52 (1995) 35-38. https://doi.org/10.1103/PhysRevB.52.35

[8] L. Zeng, L. Tan, *J. Alloys Compd*. 346 (2002) 197-199. https://doi.org/10.1016/S0925-8388(02)00522-4

[9] M. Zelinska, O. Zhak, S. Oryshchyn, V. Babizhetskyy, J.-I. Pivan, R. Guérin, *J. Alloys Compd.* 437 (2007) 133-139. https://doi.org/10.1016/j.jallcom.2006.07.087

[10] V.V. Romaka, L. Romaka, A. Horyn, P. Rogl, Yu. Stadnyk, N. Melnychenko, M. Orlovskyy, V. Krayovskyy, *J. Solid State Chem*. 239 (2016) 145-152. https://doi.org/10.1016/j.jssc.2016.04.029

[11] V.V. Romaka, L. Romaka, A. Horyn, Yu. Stadnyk, *J. Alloys Compd.* 855 (2021) 157334-11. https://doi.org/10.1016/j.jallcom.2020.157334

[12] W. Kraus, G. Nolze, POWDER CELL – a program for the representation and manipulation of crystal structures and calculation of the resulting X-ray powder patterns, *J. Appl. Crystallogr.* 29 (1996) 301-303. https://doi.org/10.1107/S0021889895014920

[13] L. Akselrud, Y. Grin, *J. Appl. Crystallogr*. 47 (2014) 803-805. https://doi.org/10.1107/S1600576714001058
[14] M.N. Abdusalyamova, O.I. Rachmatov, *J. Alloys Compd.* 299 (2000) L1-L3. https://doi.org/10.1016/S0925-8388(99)00581-2
[15] M.N. Abdusalyamova, N.A. Vlasov, Y.M. Goryachev, *Inorg. Mater.* 20 (1984) 1242-1245.
[16] T.B. Massalski, *Binary Alloys Phase Diagrams*, ASM International, Metals Park, Ohio, 1990.
[17] H. Okamoto, *Phase Diagrams for Binary Alloys*, Materials Park (OH): ASM, 2000.
[18] K.H.J. Buschow, *J. Less-Common Met.* 16 (1968) 45-43. https://doi.org/10.1016/0022-5088(68)90155-0
[19] K.H.J. Buschow, A.S. Van Der Goot, *J. Less-Common Met.* 22 (1970) 419-428. https://doi.org/10.1016/0022-5088(70)90129-3
[20] G. Vogl, M. Kaisermayr, O.G. Randl, *J. Phys. Condens. Matter* 8 (1996) 4727-4738. https://doi.org/10.1088/0953-8984/8/26/005
[21] Y.A. Mozharivskyj, Y.B. Kuz'ma, *J. Alloys Compd.* 236 (1996) 203-205. https://doi.org/10.1016/0925-8388(95)02093-4
[22] E.L. Thomas, M. Moldovan, D.P. Young, J.Y. Chan, *Chem. Mater.* 17 (2005) 5810-5816. https://doi.org/10.1021/cm051196a
[23] W.K. Hofmann, W. Jeitschko, *J. Less-Common Met.* 139 (1988) 313-322. https://doi.org/10.1016/0022-5088(88)90119-1
[24] S. Stoyko, O. Zhak, S. Oryshchyn, V. Babizhetskyy, K. Hiebl, *J. Alloys Compd.* 602 (2014) 1-7. https://doi.org/10.1016/j.jallcom.2014.02.184